How to cite: *Angew. Chem. Int. Ed.* **2022,** *61,* e202112959
International Edition: doi.org/10.1002/anie.202112959
German Edition: doi.org/10.1002/ange.202112959

VIP Fluorescent Probes | Very Important Paper | Hot Paper

Linker Molecules Convert Commercial Fluorophores into Tailored Functional Probes during Biolabelling

Lei Zhang[+], Michael Isselstein[+], Jens Köhler[+], Nikolaos Eleftheriadis, Nadia M. Huisjes, Miguel Guirao-Ortiz, Alessandra Narducci, Jochem H. Smit, Janko Stoffels, Hartmann Harz, Heinrich Leonhardt, Andreas Herrmann, and Thorben Cordes**

Abstract: Many life-science techniques and assays rely on selective labeling of biological target structures with commercial fluorophores that have specific yet invariant properties. Consequently, a fluorophore (or dye) is only useful for a limited range of applications, e.g., as a label for cellular compartments, super-resolution imaging, DNA sequencing or for a specific biomedical assay. Modifications of fluorophores with the goal to alter their bioconjugation chemistry, photophysical or functional properties typically require complex synthesis schemes. We here introduce a general strategy that allows to customize these properties during biolabelling with the goal to introduce the fluorophore in the last step of biolabelling. For this, we present the design and synthesis of 'linker' compounds, that bridge biotarget, fluorophore and a functional moiety via well-established labeling protocols. Linker molecules were synthesized via the Ugi four-component reaction (Ugi-4CR) which facilitates a modular design of linkers with diverse functional properties and bioconjugation- and fluorophore attachment moieties. To demonstrate the possibilities of different linkers experimentally, we characterized the ability of commercial fluorophores from the classes of cyanines, rhodamines, carbopyronines and silicon-rhodamines to become functional labels on different biological targets in vitro and in vivo via thiol-maleimide chemistry. With our strategy, we showed that the same commercial dye can become a photostable self-healing dye or a sensor for bivalent ions subject to the linker used. Finally, we quantified the photophysical performance of different self-healing linker–fluorophore conjugates and demonstrated their applications in super-resolution imaging and single-molecule spectroscopy.

Introduction

Fluorescence techniques are indispensable tools at the heart of basic research, imaging,[1] medical diagnostics,[2] cancer research,[3] personalized medicine and drug screening.[4] Their merits are often not limited by physical instrumentation (e.g., detectors, light sources, filters etc.), but by the performance and properties of the employed fluorescent probes,[5] i.e., light-absorbing and emitting organic molecules or proteins. Many commercially available synthetic organic fluorophores (or dyes) suffer from various shortcomings: often they are dim, undergo fast signal loss and cause phototoxicity.[6–11] For certain applications, they need functional properties including blinking emission,[7] sensor capabilities[5,8] or high photostability.[9] Functional fluorophores with favorable photophysical properties can be

[*] Dr. L. Zhang,[+] M. Isselstein,[+] N. M. Huisjes, A. Narducci, Prof. Dr. T. Cordes
Physical and Synthetic Biology, Faculty of Biology,
Ludwig-Maximilians-Universität München
Großhadernerstr. 2–4, 82152 Planegg-Martinsried (Germany)
E-mail: cordes@bio.lmu.de

Dr. L. Zhang[+]
Institute of Advanced Synthesis,
School of Chemistry and Molecular Engineering,
Nanjing Tech University
Nanjing 211816 (China)

Dr. J. Köhler,[+] J. Stoffels, Prof. Dr. A. Herrmann
(DWI) Leibniz Institute for Interactive Materials,
Forckenbeckstr. 50, 52056 Aachen (Germany)
and
& Institute of Technical and Macromolecular Chemistry,
(RWTH) Aachen University, Worringerweg 2,
52074 Aachen (Germany)
E-mail: herrmann@dwi.rwth-aachen.de

Dr. N. Eleftheriadis, N. M. Huisjes, Dr. J. H. Smit, Prof. Dr. T. Cordes
Molecular Microscopy Research Group, Zernike Institute for Advanced Materials, University of Groningen,
Nijenborgh 4, 9747 AG Groningen (The Netherlands)

M. Guirao-Ortiz, Dr. H. Harz, Prof. Dr. H. Leonhardt
Human Biology & Bioimaging, Faculty of Biology,
Ludwig-Maximilians-Universität München, Großhadernerstr. 2–4,
82152 Planegg-Martinsried (Germany)

[+] These authors contributed equally to this work.

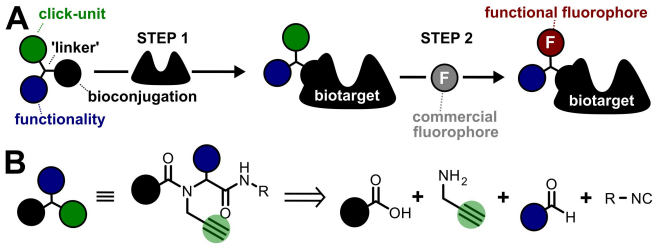

Figure 1. A) Schematic representation of the linker biolabelling strategy consisting of two steps: bioconjugation of the linker to a biotarget (e.g., for protein labeling via cysteine-maleimide chemistry) and subsequent fluorophore attachment to the complex, e.g., via click-chemistry. B) Retrosynthetic analysis of a possible linker structure.

obtained from linear multistep synthesis by coupling commercial fluorophores to new functional moieties[10] or by modification of the fluorophore core.[11] In both cases the diversification of properties requires selection of the fluorophore prior to synthesis. The use of the resulting optimized and functional fluorophore is unfortunately often limited to specific applications, e.g., for lipid-staining,[12] organelle marking,[13] DNA sequencing,[14] super-resolution imaging,[15] single-molecule detection,[9a,16] or expansion microscopy,[17] to name only a few. After purchase, fluorophore properties or bioconjugation chemistry cannot be modified without major synthetic efforts, which may consume large amounts of expensive commercial fluorophores.[9c,10a,18]

The goal of this work was to overcome these obstacles and to introduce new properties to commercial fluorophores during biolabelling. This allows fluorophore and functionality selection at much later stages close to the actual application. Our approach is based on a central "linker" compound that allows selective labeling of biological targets with a commercial fluorophore, which becomes tuneable in its properties via the linker (Figure 1A).

Herein, we describe the design and synthesis of linker compounds (Figure 1B) that comprise the required distinct moieties for functionality, selective bioconjugation and attachment of commercial fluorophores. Bioconjugation of the linker and fluorophore attachment are based on well-established linking chemistries (NHS esters, maleimides, click chemistry or via tags) and can be combined with existing protocols for labeling with commercial fluorophores (Figure 1A). By retrosynthetic analysis of possible linker structures, the Ugi-4CR reaction[19] was identified as method of choice for their synthesis (Figure 1B). The Ugi-4CR relies on the reaction between an aldehyde, an amine, an isocyanide, and a carboxylic acid in one-pot to obtain α-*N*-acetoamido carboxamide derivatives (Scheme 1). The reaction is straightforward, atom-efficient, cost-effective, and usually produces the desired adducts with high selectivity. With these features, the Ugi-4CR reaction has become the most important isocyanide-based multicomponent reaction to access peptide-like structures and has been widely applied in organic-[20] and medicinal chemistry,[21] including bioconjugation.[22] In the context of chromophores, it was employed for the generation of functional dyes and polymers.[23] To the best of our knowledge, it has never been

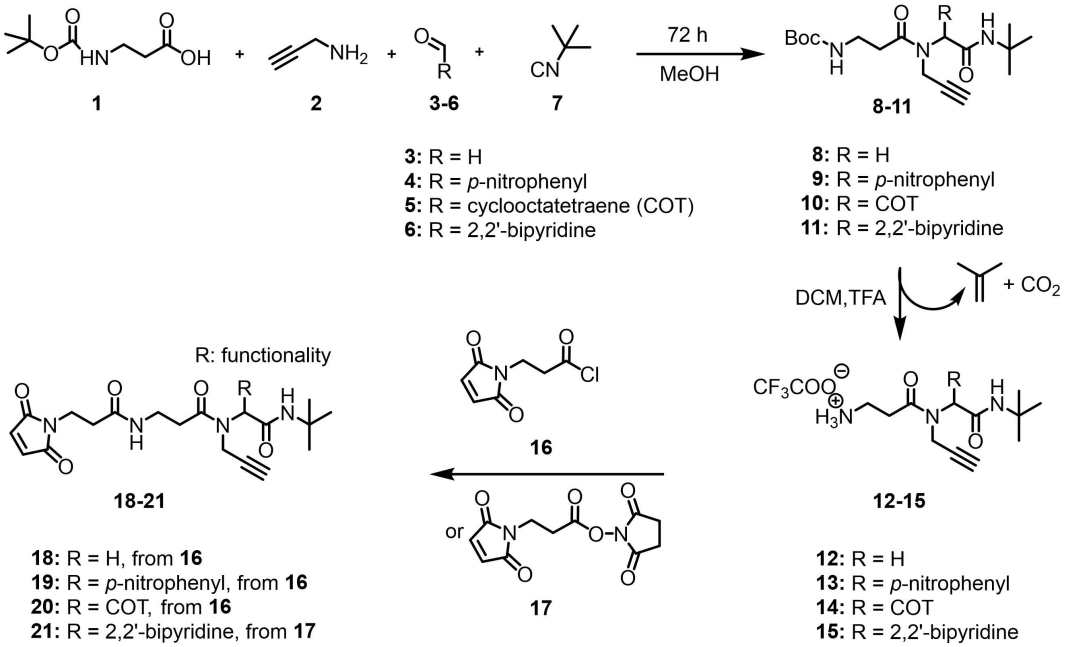

Scheme 1. Synthesis route to linker compounds with photostabilizers (**19**, **20**) or a metal-chelating unit (**21**) as functional moiety. Compound **18** lacks a functional moiety and was synthesized as a negative control. Boc protection of compounds **8**–**11** was removed in the form of 2-methylpropene and carbon dioxide under acidic conditions, yielding **12**–**15**. DCM, dichloromethane; TFA, trifluoroacetic acid; Boc, *tert*-butyloxycarbonyl.

employed for the fabrication of multifunctional linker molecules that tailor the optical properties of adjacent fluorophores. The modularity of Ugi-4CR allows the exchange of functional groups in the linker, while the chemical framework is maintained. This allows systematic variations of bioconjugation site, the fluorophore tag or the functional moiety of the linker (Figure 1). While there are other trifunctional linkers described in the literature by us for self-healing dyes,[9c] the Hofkens lab for expansion microscopy[17b,c] and others,[10a] these require the full assembly of the functional dye before labeling. We thus believe that our concept will be of great importance for many groups in biology, biochemistry and biophysics who are eager to obtain functional fluorophores or modify other properties during biolabelling.

Here, we demonstrate the selective and efficient bioconjugation possibilities of our linker strategy (Figure 1) by fluorophore attachment to proteins, nucleic acids, nanobodies in vitro and cellular targets via linkers with different functional groups. We show that two distinct functional properties can be imposed onto the same commercial cyanine dye (sulfo-Cy5, sCy5) via variation of the functional group of our linker: i) increased photostability making the dye "self-healing" or ii) sensing of bivalent metal ions by reversible binding to a chelating bipyridine unit. Furthermore, we characterize photophysical parameters of selected self-healing linker-fluorophore conjugates based on fluorophores from the classes of cyanines, rhodamines, carbopyronines and silicon-rhodamines on double-stranded DNA and a substrate binding protein of a membrane transporter. Finally, we demonstrate the durable performance of self-healing linker-conjugates of ATTO647N for improved data acquisition in diffusion-based single-molecule Förster resonance energy transfer experiments, where the linker diminishes photophysical artifacts, as well as in confocal and super-resolution STED-imaging involving fixed HeLa-cells.

Results

For the biolabelling strategy (Figure 1A), we aimed at obtaining linker molecules (Figure 1B) that allow a straightforward combination of at least three different chemical groups, which can be altered by a mere change of starting materials. The linker structures studied (Scheme 1, compounds **18**–**21**) were designed to contain the following chemical moieties: A maleimide-group to attach the linker to sulfhydryl-groups present in biological targets, a functional moiety R and an alkyne-group that allows bioorthogonal copper-based click-chemistry for fluorophore attachment. We investigated three different types of functional groups, i.e., i) hydrogen as a non-functional negative control (**18**), ii) the photostabilizers *p*-nitrophenyl (NP, **19**) and cyclooctatetraene (COT, **20**), and iii) a metal-chelating unit (2,2′-bipyridine, **21**).

Considering the structures of desired reaction products **18**–**21** (Figure 1/Scheme 1) and the commercial availability of reagents, we chose acid **1** as an anchor for the bioconjugation site, an amine-functionalized alkyne-unit **2** for click-chemistry and aldehyde derivatives **3**–**6** bearing the different functional groups (Scheme 1). All starting materials were commercially available except for compounds **5, 6** and **16**, which were synthesized (for details see Supporting Information Part I/II, Figure S2–S5, S18). The mixture of four components, i.e., **1**, **2**, **7** in combination with either **3**–**6**, reacted in methanol over 48–72 h to yield α-*N*-acylamino amides **8**–**11** with reaction yields of 73–87 % for **8**, **9**, **11** and 49 % for **10**. Compounds **8**–**11** were purified and fully characterized (for details see Supporting Information, Part I/II, Figure S6–S11, S19, S20). Subsequently, the Boc-protecting group was removed via addition of TFA and the crude products **12**–**15** were used in the reaction with **16** or **17** without any further purification. The linker molecules **18**–**21** were isolated and purified via column chromatography on the 100–300 mg scale at yields of 25–81 % (0.23, 0.36, 0.40, 1.14 mmol respectively, for details see Supporting Information, Part I/II, Figure S12–S17, S21, S22, S25–S28).

We next assessed the ability of compounds **18**–**21** to serve as linkers between a commercial fluorophore and different biological targets in vitro and in vivo (Figure 2A). This was done in a realistic context, i.e., we integrated the linker into well-established labeling procedures of proteins, nucleic acids and live bacteria (Figure 2A). In our protocol, we first attached **18**–**21** to sulfhydryl residues in the respective targets as shown schematically in Figure 1A (for details see Supporting Information, Part III). Once the linker was bound to the target, a commercial fluorophore was introduced via a bio-orthogonal click reaction with the alkyne-moiety present on the linker. For the latter, we chose the Cu^{I}-catalyzed alkyne-azide cycloaddition (CuAAC)[24] since it is a very selective and efficient bio-orthogonal reaction, for which a wide variety of azide-functionalized fluorophores are commercially available. Furthermore, the formed triazole adduct is known to be stable against hydrolytic cleavage or redox reactions under physiological conditions.[25] Importantly, all labeling steps were done without advanced purification methods, which were required in our previous work on self-healing dyes that we based on an unnatural amino-acid scaffold.[9c]

We used the isolated substrate-binding domain SBD2 of the ABC transporter GlnPQ as our first test system.[26] To this end, we produced a single-cysteine variant of the protein (SBD2-T369C, details see Supporting Information, Figure S30), which was labeled using commercial maleimide derivatives of sulfo-Cy3 (sCy3), TMR, sCy5 and ATTO647N. For this, the protein was first immobilized on a Ni^{2+}-Sepharose resin, subsequently incubated with the corresponding fluorophore-maleimide and eluted. Excess fluorophore was removed via gel-filtration chromatography. The eluent solution showed co-migration of protein and fluorophore via corresponding absorbance in the UV (280 nm for the protein) and visible absorption (for the dye). With this strategy, we obtained labeling efficiencies between 60–70 % for direct labeling with different commercial maleimide dyes, derived from a comparison of the molar concentrations of protein and dye (Figure 2C); for details see Material and Methods in the Supporting Information, Part III.

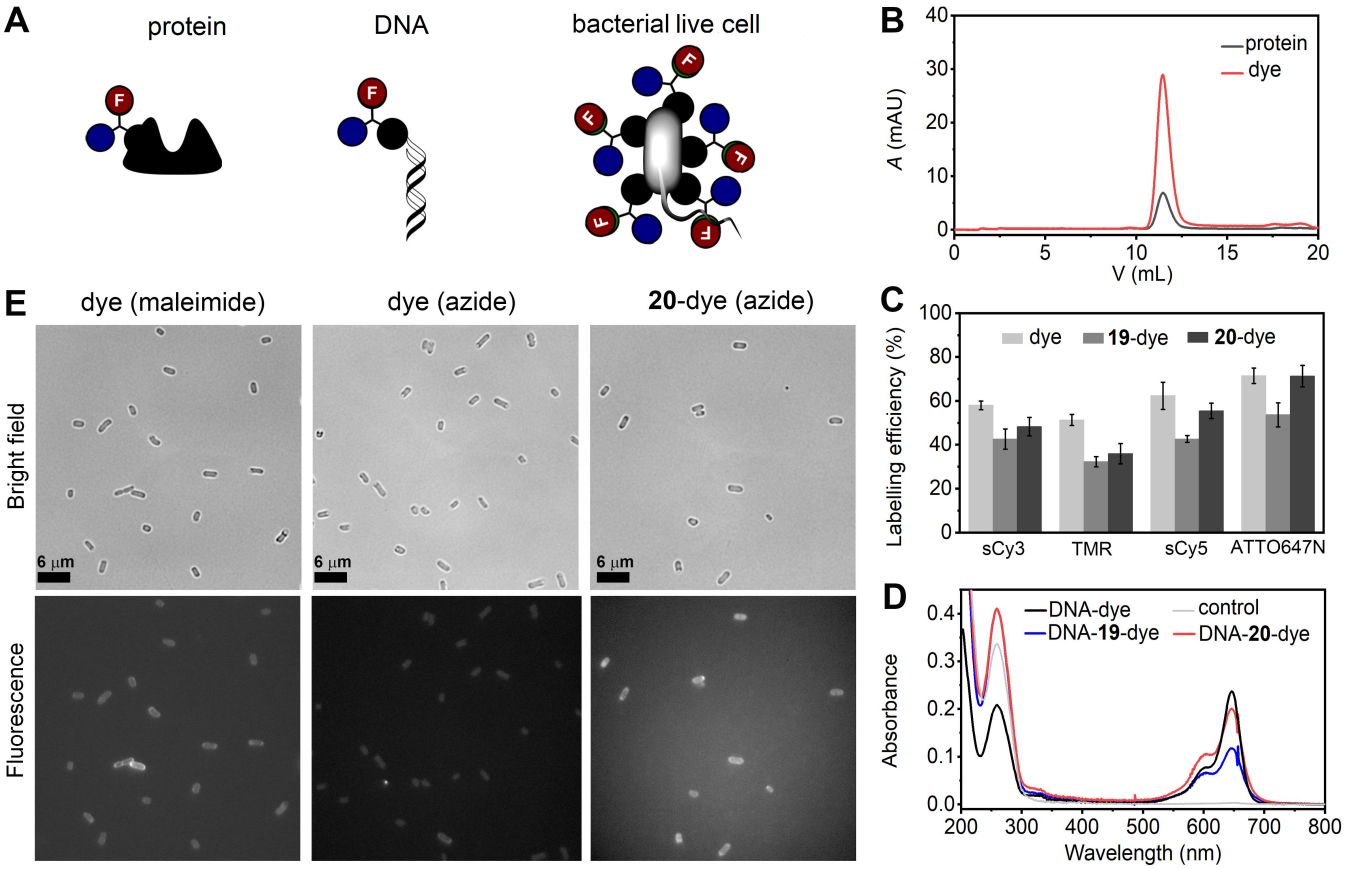

Figure 2. Labeling performance of linker molecules **19** and **20** on different biotargets in comparison to commercially-available maleimide fluorophore derivatives. A) Schematic view of biotargets and attachment strategy shown in the Figure. B) SEC-image of a successful labeling procedure of SBD2-T369C labeled with **19**-sCy5. The black curve shows absorption at 280 nm (protein absorbance) and the red curve shows absorption at 647Nm (sCy5 absorbance maximum). Comparison of the area below the elution profiles allowed to determine labeling efficiencies in (C) considering the extinction coefficient of the protein and the published values of the respective dyes (see Supporting Information, Part III for details). C) Quantitative comparison of the labeling efficiency of SBD2-T369C with either maleimide-functionalized fluorophore (protein-maleimide dye) or with azide-functionalized fluorophore clicked by **19** (protein-**19**-dye) or **20** (protein-**20**-dye). D) UV/Vis absorbance spectra showing the characteristic bands for dsDNA (≈260 nm) and the respective fluorophores (≈650 nm, data shown for sCy5). Control indicates that the labeling procedure of azide-functionalized fluorophore was conducted in the absence of a linker. E) Brightfield and fluorescence microscopy images of live bacteria (*E. coli* K12), which were labeled with maleimide-functionalized Cy3B (left column), azide-functionalized Cy3B in the absence of a linker (middle column) and azide-functionalized Cy3B clicked by compound **20** (right column).

Alternatively, we treated SBD2 first with the linker compounds **19** or **20**, washed and subsequently incubated with azide fluorophores and copper-catalyst. Figure 2B shows a typical SEC-chromatogram of successful SBD2-labeling by a linker-fluorophore conjugate with a monodisperse peak showing protein and dye absorbance signals (280 nm, protein and 650 nm, dye) with an elution volume of ≈11 mL matching SBD2.[26] To exclude unspecific labeling of the dyes, we performed a control experiment without linker. We observed no labeling as deduced from missing visible fluorophore absorbance (Figure S32 and S36). Next, we compared the overall labeling efficiencies of both approaches, i.e., direct maleimide labeling of SBD2 and labeling via compound **19** or **20** (Figure 2C and Figure S33) for commercially available cyanine (sCy3/sCy5), rhodamine (TMR) and carbopyronine (ATTO647N) fluorophores. The overall labeling efficiency was lower for the **19**-fluorophore combinations but like direct labeling of commercial maleimide dyes for all **20**-fluorophore combinations. We also tested a simplified synthetic scheme for a smaller linker compound **22** (Figure S34) with a nitrophenyl-functional group, where the maleimide is replaced by an acrylamide-group (see also Supporting Information, Part I/II, Figure S23, S24 and S29). Again, with this molecule we could link sCy5 to SBD2 via a light-induced thiol-acrylamide Michael addition[27] (Figure S34). All these experiments demonstrate that protein labeling with commercial fluorophores via linkers **19** and **20** is selective, shows a high labeling efficiency and only occurs when the linker compounds were attached to the cysteine residue on the protein prior to fluorophore addition.

Similar labeling was achieved for double-stranded DNA (dsDNA) containing a terminal thiol-group (Figure 2D). After incubation of the thiol-containing dsDNA with linker, the conjugates were labeled via click-chemistry with fluorophores and purified with PD-10 desalting columns after

each step. Resulting adducts were characterized by UV/Vis absorption spectroscopy (Figure S35). The UV/Vis spectra display the absorption maxima for dsDNA (≈260 nm) and the respective fluorophores of the dyes, e.g., for red dyes at ≈650 nm (Figure 2D and Figure S35). As a control, direct labeling of dsDNA by the azide-functionalized fluorophores in the absence of the linker gave no characteristic peak for the dyes (grey "control" curves in all absorbance spectra in Figure 2D and Figure S35).

Finally, we tested compound **20** for membrane labeling of accessible thiols in living *E. coli* K12 cells. To this end, cells were grown on microscope coverslips and incubated with maleimide-functionalized Cy3B to obtain outer-membrane staining.[28] Cells showed homogeneous labeling seen by a comparison of bright field and fluorescence images using an epi-fluorescence microscope (Figure 2E, dye-(maleimide)). We next demonstrated linker-specific labeling of the cells (Figure 2E, **20**-dye (azide)). The addition of compound **20** as a linker between dye and outer membrane thiols resulted in brighter cells in comparison to control experiments, where cells were only incubated with azide-functionalized Cy3B but no linker (Figure 2E, dye (azide)).

After successfully establishing the linker biolabelling strategy for different in vitro and in vivo targets, we tested whether the functionality of commercial dye molecules could be altered based on the available linker structures with distinct chemical moieties (Figure 3). We selected two different linker functionalities, i.e., intramolecular triplet-quenching via cyclooctatetraene (COT) and fluorophore quenching via PET using 2,2′-bipyridine as unit for rever-

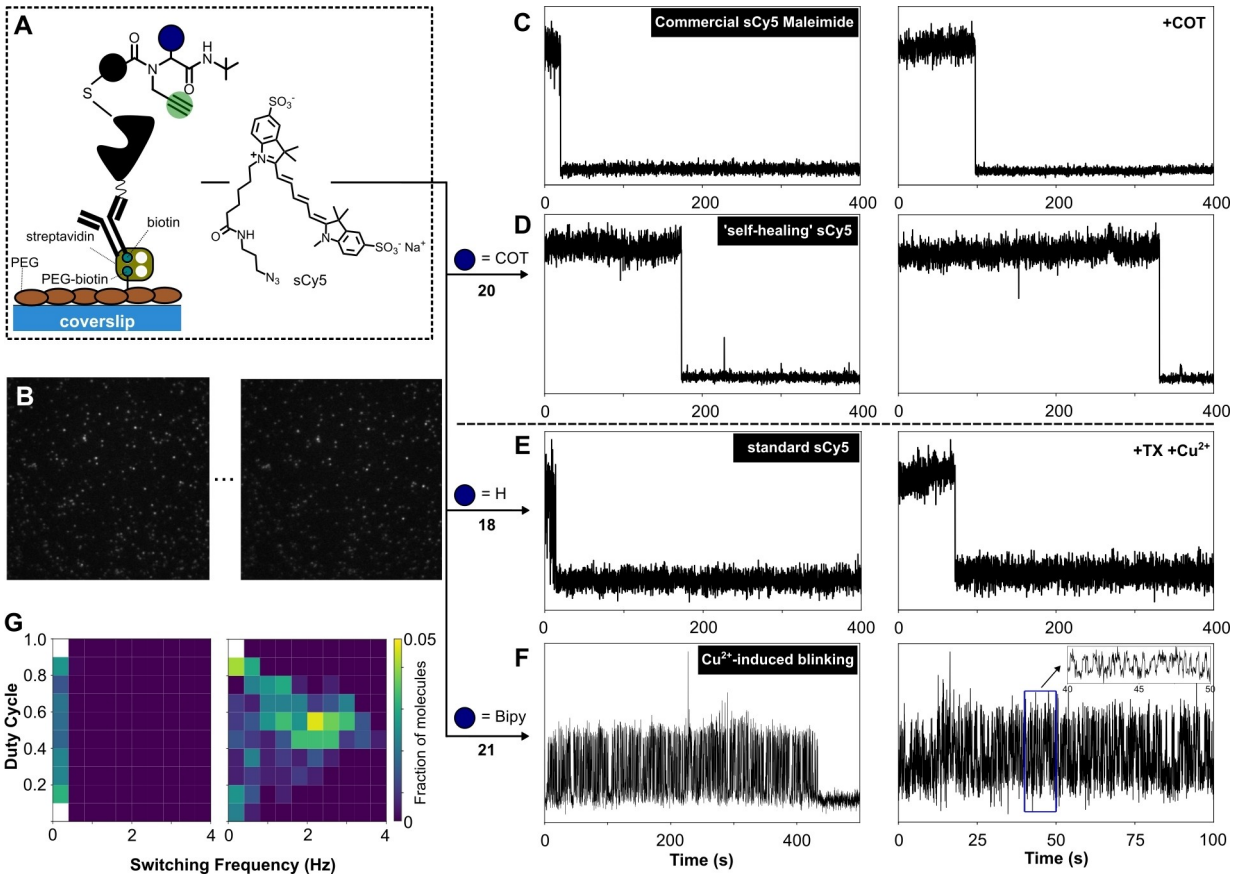

Figure 3. Proof-of-concept experiments to demonstrate the ability of the linker to equip commercial sCy5 with self-healing or blinking properties on model protein SBD2. A) Schematic view of protein surface immobilization strategy and linker/dye attachment. B) TIRF microscopy images show individual sCy5 molecules at the start of the movie and after 30 s (related to self-healing sCy5). C)–F) Single-molecule fluorescence time traces of (C) commercial sCy5 directly linked to SBD2 via maleimide and sCy5-azide dyes linked to SBD2 via (E) **18**, (D) **20** and (F) **21**. C, D) Comparison of photostabilization between commercially available sCy5 maleimide without photostabilizer (C, left), with 2 mM COT in solution (C, right) and **20** in the absence of photostabilizer in solution, respectively under deoxygenated conditions using POC in PBS buffer at pH 7.4; see Methods for Details. E, F) Photoblinking induced by combination of **21** and Cu^{2+}. E) Negative control of compound **18** in the absence of photostabilizer (left) and in buffer solution containing 2 mM TX and 5 μM $CuSO_4$ (right). F) Fluorescent transients of sCy5 linked via **21** under identical buffer conditions as in (E, right). E, F) Were recorded in MOPS buffer at pH 7.0 using PCA/PCD for oxygen removal with 100 ms (E/F, left) and 20 ms (F, right) exposure times, respectively. G) Quantitative blinking properties of sCy5 in the presence of 5 μM $CuSO_4$ on linker **18** (left) and on linker **21** (right). Values of the three white fields in the left panel are 0.7122 and 0.1171, and 0.1125 in the right panel, from top to down, respectively. (F, left) recorded at 100 ms and (F, right) recorded at 20 ms exposure time for clearer characterization of blinking behavior. For a direct comparison of blinking behavior between **18** and **21** under identical exposure times in presence and absence of $CuSO_4$, see Figure S37, Figure S38 and Figure S39. All measurements were done with 640 nm laser excitation with a power density of ≈150 $W\,cm^{-2}$.

sible metal-chelation. We chose these, because they represent well-characterized chemical units with known and well understood effects on fluorophores.[29] To show their effects in the context of the linker, we chose compounds **18**, **20**, and **21** to demonstrate that commercial sCy5 (Figure 3A) can become self-healing when connected via compound **20** or show copper-induced blinking when linked via compound **21**. All dye-protein constructs were investigated by TIRF-microscopy (Figure 3B), which allowed the photophysical behavior of many individual molecules to be studied in parallel.[29a]

As shown, linkage of commercial sCy5 maleimide (Figure 3C (and S44) or compound **18** (Figure 3E and S37) on a model protein resulted in short fluorescence traces where most of the dyes had noisy signals and bleached irreversibly within a few seconds. A clear improvement of this was observed for the addition of COT or TX to the imaging buffer (Figure 3C/E, traces labeled with +COT/+TX). Linkage of sCy5 via compound **20**, which localizes a photostabilizer (COT) close to the dye, forms a self-healing **20**-sCy5 (Figure 3D/S45) with stable, long-lived fluorescence signal and high SNR. Such stable emission can be used very well for state-of-the-art applications, which require high photostability as will be shown below for **20**-ATTO647N conjugates.

Secondly, we altered the functionality of sCy5 towards metal-sensing, which was previously realized in TMR-2,2′-bipyridine-constructs using the proximity of TMR and a metal-chelating moiety on two separate single-stranded DNAs after hybridization.[29b,30] Our data in Figure 3E/F shows that Cu^{2+} induces sCy5-blinking via reversible binding to the 2,2′-bipyridine ligand. This idea is supported by control experiments where no sCy5-blinking is observed despite the presence of copper in solution, namely **18**-sCy5 with 5 μM Cu^{2+} (Figure 3E (right) and Figure S37B) and **21**-sCy5 with 5 μM Cu^{2+} in the presence of 10 μM EDTA (Figure S38). The analysis of the switching frequency vs. the duty cycle (Figure 3G and Figure S39) clearly indicates the impact of the linker structure and the ability of sCy5 to sense copper ions. We defined the switching frequency as the number of completed blinking cycles divided by the time until the last detected "on" state, and the duty cycle as the fraction of total "on"-time to the total time until the last detected "on" state (see methods section for a more detailed description). Based on the data we anticipate potential of a linker-containing bipyridine for future applications in super-resolution imaging (via a STORM-like method)[29b] or metal sensing.[31]

The data shown in Figure 3 outline the potential of the linker concept to alter the functionality of the very same commercial fluorophore during established biolabelling procedures. An important question is whether the linker can have additional (unwanted) impact on biochemical function of the respective biological target, as detailed in ref. [32] for fluorophores alone. Since the linkers used here have a molecular weight around 400–500 u, i.e., approximately half of that of a fluorophore, its possible impact on biochemical targets must be considered and characterized in future studies, not only in the light of an overall "larger" fluorophore, but also in relation to an increased hydrophobic character of the construct.

To assess possible applications and the impact of our labeling strategy, we next focused on characterization of self-healing linker-dye conjugates. We decided to focus on these (and not those of the metal-sensing dyes) since we can benchmark the quantitative performance of the linker-dye conjugates better in the context of our previous work[9b,c,29a,33] and that of others.[18,34] We further reasoned that successful self-healing linker-dye conjugates would be able to fill an important gap in the field, since only very few commercial solutions are available for self-healing dyes. Blanchard and co-workers sell a selected number of self-healing cyanine dyes (www.lumidynetechnologies.com), but there is so far no commercial solution to use self-healing dyes easily on different biotargets or for other dye classes. So far, self-healing dyes are always pre-modified with a photostabilizer for biolabelling and the only flexible scaffolding approach that allows use of other dye classes requires sophisticated synthesis and dye modification,[9c] which is not accessible to most user groups. As will be shown below, the linker molecules **19/20** could fill this important gap in the field of self-healing dyes[29a] since the labeling strategy relies on the use of commercially available fluorophores and can be integrated into established labeling protocols (see Figure 1). Thus, any commercial fluorophores with click-chemistry groups could be tested with photostability-functionalities that are available on linker structures.

Figure 4 shows a quantitative characterization of photophysical parameters of dyes commonly used for single-molecule and super-resolution microscopy. The parameters of self-healing ATTO647N- and sCy5-linker conjugates were characterized on both proteins and DNA in deoxygenated buffer. We compared the performance of the self-healing dyes against the gold-standard of intermolecular photostablization by solution additives (Trolox, +TX or COT, +COT) with commercially available maleimide-linked dyes (ATTO647N and sCy5). In our analysis of TIRF movies we considered four parameters of individual fluorophores on their respective biotarget (Figure 4A): dye brightness (photon rate in kHz), total number of emitted photons (N_{total}), signal-to-noise ratio (SNR) and photobleaching lifetime (τ_B).

Both dyes in combination with the linker compounds **19/20** showed increased photo- and signal-stability in comparison to the reference dyes based on direct maleimide linkage (Figure 4). For completeness, we also assembled **18**-dye combinations in absence of photostabilizer, which showed similar performance as compared to the directly linked maleimide dyes (Figure S37A/41C).

For ATTO647N all photophysical parameters were improved for both **19**- and **20**-ATTO647N compared to the parent fluorophore (Figure 4B). While there were only moderate increases for count-rate and SNR, the photobleaching time increased strongly for **20**-ATTO647N (see Supporting Movie 1) and in a moderate way for **19**-ATTO647N in comparison to the directly linked ATTO647N (Figure S40/S42). Strikingly, the photobleaching

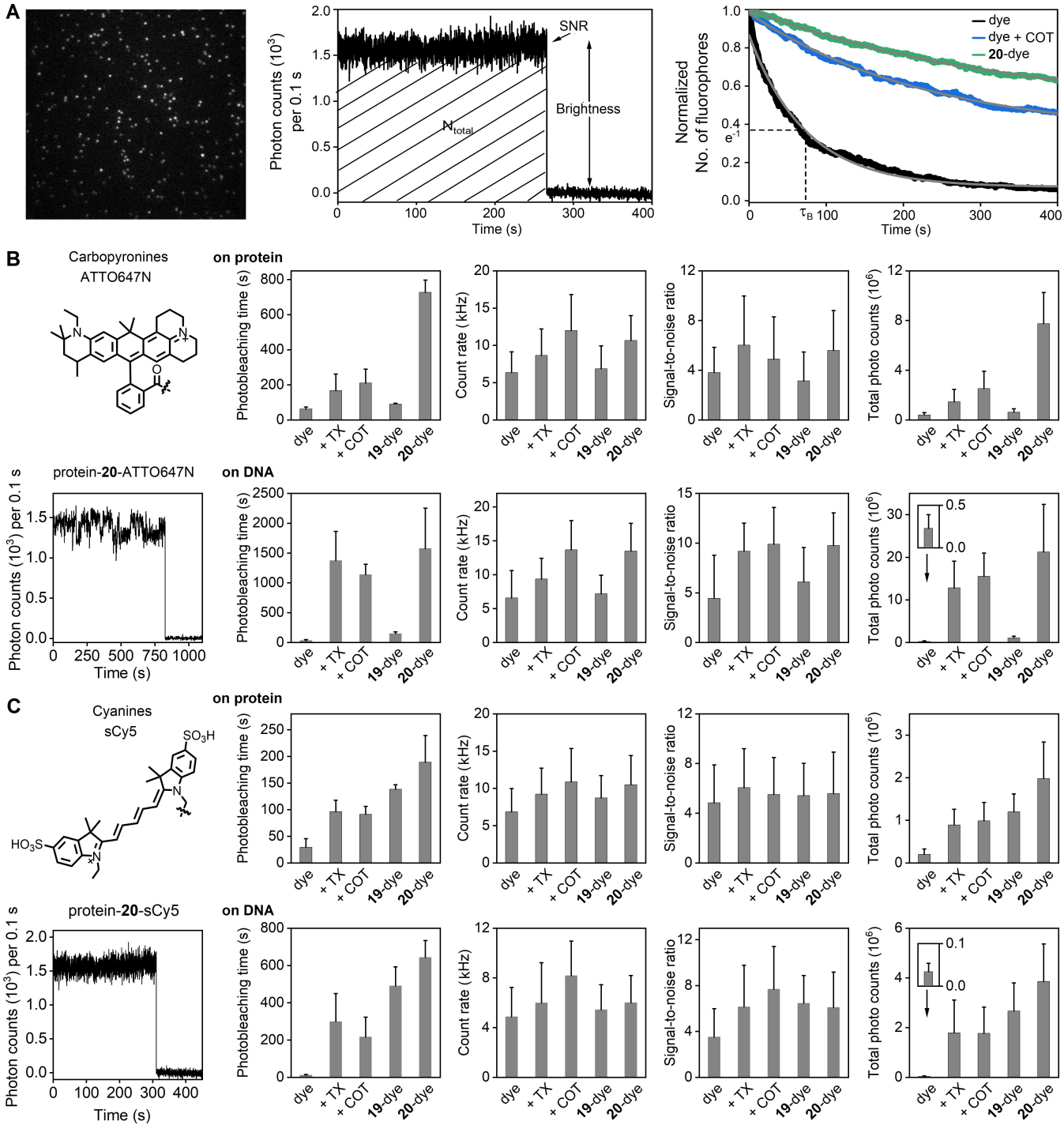

Figure 4. Photophysical characterization of biotargets containing **19**/**20**–dye conjugates with single-molecule TIRF microscopy. Data was recorded in aqueous buffer at pH 7.4 in the absence of oxygen (POC) under continuous 640 nm excitation with ≈75 W cm^{-2}. A) Representative image frame (left panel) showing single fluorescent molecules (10×10 µm, exemplarily for ATTO647N). Subsequent images recorded over a period of 450 s showed an exponential decrease in the number of fluorescing molecules with a photobleaching lifetime τ_B as shown for SBD2-ATTO647N (black, fitted in grey). The curves shown were obtained by averaging over 4 TIRF movies. The photobleaching times of **20**-ATT0647N on SBD2, ATTO647N +TX, ATTO647N + COT, **20**-ATTO647N on DNA are inaccurate and underestimated due to large fraction of fluorophores that did not show bleaching over the course of the experiment. B), C) Left panel: chemical structures and right panel: respective photophysical parameters obtained from background-corrected fluorescence traces for ATTO647N (B, carbopyronines) and sCy5 (C, cyanines) on SBD2 protein or double strand DNA (hybridization of P1 with P2, sequences shown in the Supporting Information). Values and error bars (s.d.) in bar graphs obtained from >400 molecules. For further details of the experimental techniques, data acquisition and analysis, see the Methods section.

and total number of observed photons of **20**-ATTO647N exceed that of the commonly-used buffer systems to 8×10^6 total photons on proteins and 2×10^7 total photons on dsDNA, respectively. We should highlight that for **20**-ATTO647N on proteins and DNA the photobleaching was so slow that the photobleaching time could not be determined accurately even in 30 minute long movies. So, we assume that the reported photobleaching times are underestimated.

We also observed positive effects for the photostability of sCy5 (Figure 4C) and a commercially available silicon-rhodamine fluorophore (Figure S48, SiR) developed by Johnsson and co-workers[11e] that we combined with either **19** or **20**. For sCy5 both stabilizers performed equally well as compared to solution-based healing (Figure S44/S46). Detailed data sets for all conditions for linker-dye conjugates of ATTO647N, sCy5 and SiR are provided in Figure S41 and S45 (for proteins) as well as Figure S43, S47 and S48 (for dsDNA).

In summary, we find very good photophysical performance of our linker-dye conjugates rendering them useful self-healing dyes for future applications. Strikingly, **20**-ATTO647N shows the unique features of higher photostability in comparison to solution additives, which was so far only realized for a handful of intramolecular dye-photostabilizer combinations.[18,33d,34d,e] Additionally, the approach presented allows to assemble a self-healing dye on a biomolecular target via a simple labeling procedure. We thus believe that it will find wide-spread use, provided that the linker compounds become commercially available, which is planned in the near future.

Finally, we tested **20**-ATTO647N in two state-of-the-art applications. First, we removed acceptor bleaching artifacts in diffusion-based smFRET experiments on nucleic acids (Figure 5A/B) and secondly used the high resistance to photobleaching of **20**-ATTO647N in confocal and STED-microscopy via nanobody labeling (Figure 5C–H).

For demonstration of positive effects of linker compounds in smFRET, we selected a dsDNA sample that is frequently used in the lab for calibration purposes, where strong acceptor-bleaching is present for Cy3B/ATTO647N. Microsecond alternating laser excitation was used to identify different sub-populations in our experiments: i) donor-only molecules (high S*, low E*), ii) donor–acceptor molecules (intermediate S*, high E*), and iii) acceptor-only (low S*, broad E*). Dye artifacts such as blinking or photobleaching appear as bridges between the corresponding populations in our histogram (Figure 5A, bottom). For our analysis we focused on region i/ii corresponding to an S*-range of 0.3–1.0 (full data sets for all conditions shown in Figure S49). For an inter-dye separation of 13 base-pairs (Figure 5A, top row), we observe $<20\,\%$ of the expected FRET population at $E^*\approx0.8$ for the dsDNA in PBS buffer. The data shows that the addition of 2 mM TX to the imaging buffer recovers the FRET population due to removal of acceptor-bleaching with a donor-acceptor population of $\approx50\,\%$. A similar result is seen for use of **20**-ATTO647N as acceptor dye, where both the 1D–E* and 2D histogram show two well-separated populations for donor-only ($E^*\approx0.15$) and donor-acceptor ($E^*\approx0.85$). A power-dependent analysis of the useful donor-acceptor containing molecules shows that this fraction decreases as a function of excitation power (Figure 5B), yet both **20**-ATTO647N and 2 mM TX show clean isolated FRET species (Figure S49) and higher donor-acceptor fractions compared to the non-stabilized dsDNA sample (Figure 5B). The data also suggest a small alteration of the Förster radius or shorter distance between both dyes for usage of **20**-ATTO647N due to the linker.

Following the findings for **20**-ATTO647N in smFRET, we tested the performance of this dye-linker combination in cellular imaging. To establish cellular staining with linker compounds we labeled a specific binder for GFP called GBP.[35] Therefore, we converted surface-accessible lysines in GBP via a commercial kit into thiols[36] and subsequently labeled the nanobodies with **20**-ATTO647N and ATTO647N (Figure S31). We then stained HeLa cells expressing GFP-αTubulin (Figure 5C) and GFP-H2B (Figure 5D) for STED and confocal imaging. We selected αTubulin as an example for structures, which can only be well-resolved by STED microscopy and histone H2B because of high nuclear expression levels. The targets thus allowed to characterize whether a certain imaging modality reaches optical resolution <250 nm with αTubulin (Figure 5C, see comparison STED/confocal). Furthermore, the H2B staining allowed us to perform systematic photobleaching studies, where we compare the signal reduction in representative 2.8×2.8 µm patches in terms of the integrated fluorescence signal (Figure 5E/G). For data analysis we normalized the intensity values of confocal and STED imaging to first frames and report the average decay times in frames for each condition. Both in confocal and STED-imaging we see a statistically significant retardation of bleaching for **20**-ATTO647N in comparison to ATTO647N (Figure 5F/H). The observed effects of compound **20** were larger for in vitro samples using TIRF microscopy (Figure 4) in comparison to cellular imaging studies via confocal and STED microscopy (Figure 5). We attribute this to differences in excitation intensity along the z-axis. In TIRF excitation all excited molecules are in an exponentially decaying evanescent field with $\approx$100–200 nm thickness with homogeneous excitation intensity. In confocal techniques, excitation extends in the z-direction over more than 500–1000 nm. Assuming a non-linear relation between excitation power and photostabilization, the protective effect of compound **20** would be highly dependent on the specific power and labeling density in confocal techniques. Furthermore, additional interactions of the fluorophores with the nanobody or redox-active molecules present in the cellular environment might also reduce the observed photostabilization effects.

Discussion and Conclusion

Many commercially available fluorophores have a limited application scope, suffer from fast signal loss, induce phototoxicity, or are confronted with the requirement for demanding functional properties. Unfortunately, there is so far no simple (commercial) solution to modify their chemical

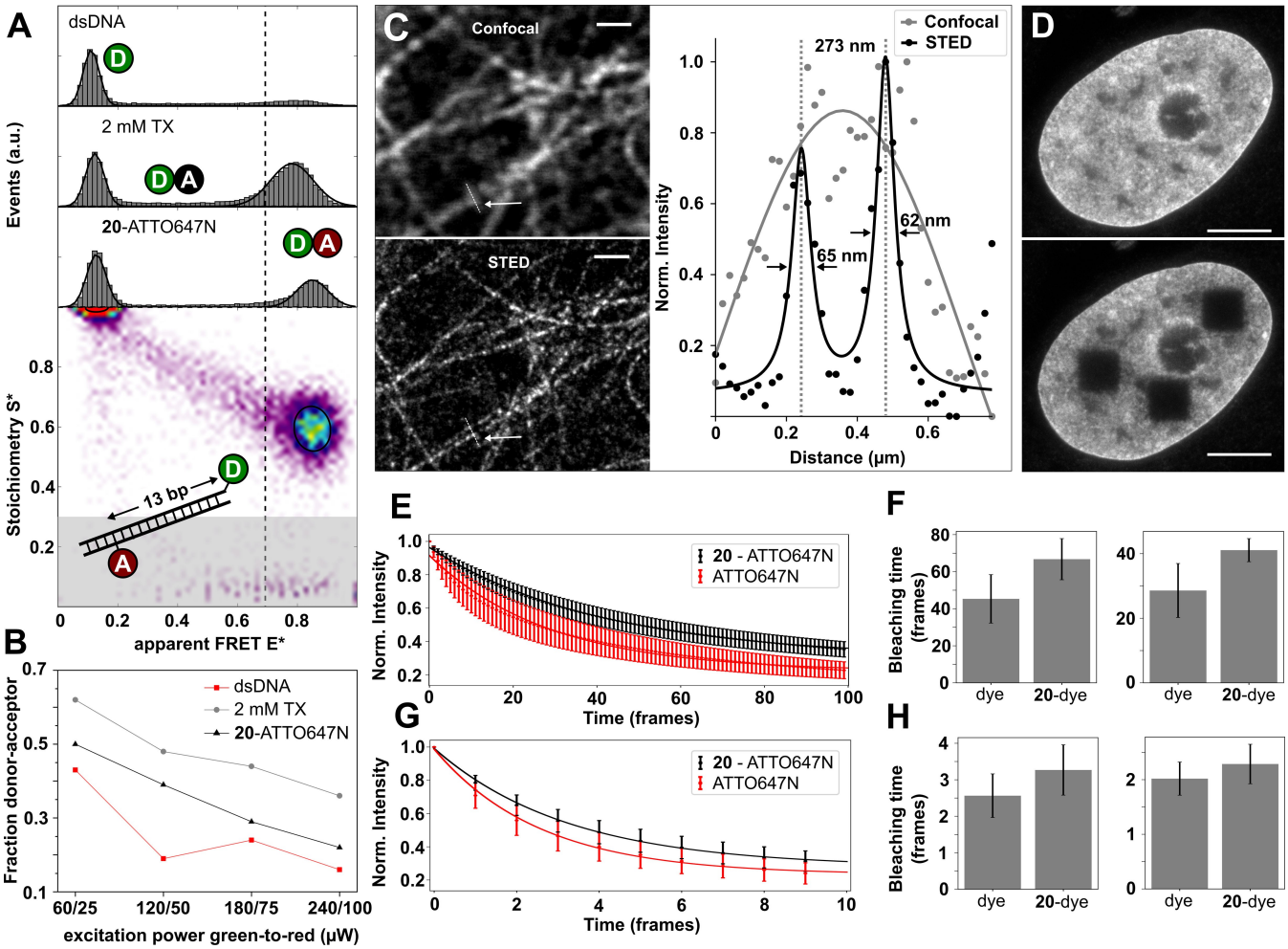

Figure 5. Applications of linker-conjugated self-healing dyes in single-molecule FRET (µsALEX) and STED super-resolution microscopy. A) 2D histograms of joint pair values of S* (labeling stoichiometry) and E* (FRET efficiency, that correlates to interprobe distance) of Cy3B (donor)/ATTO647N (acceptor) on dsDNA in the absence and presence of 2 mM TX and Cy3B (donor)/**20**-Atto647N as the acceptor in PBS pH 7.4 buffer. B) Dependence of the donor-acceptor population of the corresponding conditions in (A) for increasing excitation intensity. C, left half) confocal (top) and STED (bottom) images of tubulin stained with GFP-binder-**20**-ATTO647N in HeLa H2B-mRFP-mEGPF-αTubulin cells. Scalebar: 1 µm. (C, right half) intensity profile along the line indicated in (C top and bottom) by an arrow showing increase of resolution through STED. Lines indicate a gaussian fit for confocal (gray) and a double-Lorentzian fit for STED data (black), respectively. The fit to the STED data reveals a line distance of 273 nm and a Full Width Half Maximum (FWHM) of 65 nm and 62 nm for the resolved peaks, respectively. D)–H) Images and bleaching analysis in Hela-H2B-GFP cells stained with GFP-binder prelabeled with either ATTO647N or **20**-ATTO647N. D) Confocal images of nuclei labeled with GFP-binder-**20**-ATTO647N before (top) and after (bottom) bleaching. Scalebar: 5 µm. E)–H) Bleaching analysis from stained cells as described in the Supporting Information (Part II, Immunostaining). E), F) Under Confocal Scanning Microscopy and (G, H) under STED Microscopy conditions. E), G) Normalized fluorescent time traces with exponential fit. Error bars correspond to one standard deviation of the data. F), H) Bleaching times under 20% Confocal intensity (F, left), 50% Confocal intensity (F, right), 20% Confocal and 40% STED intensity (H, left), 50% Confocal and 40% STED intensity (H, right). Error bars in (F), (H) correspond to one standard deviation of fitted bleaching times.

properties or bioconjugation chemistry without major synthetic efforts post purchase. We here present a solution to these problems via introducing linker molecules that allow to functionalize commercial fluorophores during biolabelling which makes complex chemical modifications redundant. We believe that both our biolabelling strategy and the synthesis route of the linker are new versatile tools for biochemical- and biophysical investigations and fluorescence imaging. The biolabelling and fluorophore attachment is based on commonly used linking chemistries (NHS esters, maleimides, click chemistry) and can thus be integrated into existing protocols. With such a simple strategy, users in all branches of academic and industry research, but also in biomedicine will be able to modify properties of commercially available fluorophores preserving their standard labeling routines. The synthesis strategy of the linker molecules itself was realized with commercial precursors, is cost effective, has high yields, and consequently offers the possibility for extension into a larger linker library. Systematic variations of single components in the Ugi-4CR and post-modification approaches, which we plan in future projects, will allow to modify either the bioconjugation site, the fluorophore tag or the functional moiety of the linker molecules.

Diversification of bioconjugation aims at obtaining linkers for labeling of many relevant targets in vitro and in vivo. This could be approached by replacing activated 3-maleimidopropionic acid in the final conjugation step (Scheme 1). We believe that attachment of reactive groups for bioconjugation via strain-promoted alkyne–azide or alkyne–nitrone cycloaddition,[37] inverse-electron demand Diels–Alder reaction,[38] condensation of 1,2-aminothiol with 2-cyanobenzothiazole[39] and protein- or peptide-based tags, such as the SNAP-tag motif can be developed via a similar synthesis.[40]

Another key aspect will be diversification of the bioorthogonal attachment of the commercial fluorophore derivative to the linker for attaching a fluorophore NHS ester, sulfhydryl-groups for attaching a fluorophore maleimide, ring-strained alkynes[37] for attaching a fluorophore azide or ring-strained alkenes for attaching a fluorophore tetrazine.[38] With these most types of commercially available reactive fluorophores can be used with the linker approach. Importantly, the labeling chemistries for biological target and fluorophore attachment must be chosen such that they do not interfere with each other. It may thus be necessary to alter the two in their nature or specific position in the linker (Scheme 1), depending on the biological sample and the desired fluorophore.

From a functional viewpoint, we hope to obtain linkers in the future that can equip all kinds of commercial dyes with new functional properties such as metal-ion sensing,[29b] tailored blinking kinetics,[41] introduction of purification tags, and others. Also, bio-reactive functional dyes might be assembled directly using optimal combinations of fluorophore, functional and bio-reactive unit via the Ugi-4CR directly (as was also suggested in Ref. [23b]). For the latter, the linker approach presents a fast pre-screening method to identify the ideal combinations of fluorophore and functional group.

We believe that linkers could enable novel live-cell imaging aspects and modalities, e.g., an improvement of dyes used for STED imaging (STAR635P[33a]). They might also help to cope with the presence of molecular oxygen, i.e., to identify dye-photostabilizer combinations that show good photostability in the presence of oxygen. Furthermore, metal-chelating dyes for STORM imaging (CHIRON method[29b]) could be based on the linker. Also, the linker could help to create new self-blinking dyes for STORM where nucleophiles such as thiols or hydroxy-groups are combined with silicone rhodamine dyes.[42] Another conceptual possibility with linkers is to create double fluorophore anchoring sites, e.g., via the use of double-alkyne linkers that facilitate fluorophore-fluorophore interactions. Two fluorophore labeling sites in close proximity might be useful for creation of photoactivatable dyes previously used in STORM, i.e., to create a green/red activator combination.[43] Alternatively, two labeling sites might allow to convert the stable emission of fluorophores such as ATTO655, TMR or ATTO647N into self-blinking dyes via fluorophore–fluorophore quenching processes. The latter strategy would not require additional laser sources or buffer additives for fluorescence on/off-switching and could be a general strategy to create a new class of self-blinking dyes.

As demonstrated by Blanchard and co-workers recently,[18] self-healing dyes are particularly suited for FRET studies with high temporal resolution as high as 250 μs. With this, a direct observation of fast conformational fluctuations on the sub-millisecond time range or analysis of transition path times[44] becomes possible if sufficient count-rates (and total number of detected photons) are available. Since we demonstrated count-rates in the range of >1 MHz with self-healing based on a combination similar to **18**-ATTO647N previously,[33a] we hope to obtain FRET traces with a time binning in 10–50 μs steps using selected linker-dye combinations. These would allow to resolve fast conformational transitions in proteins for a detailed elucidation of ligand-binding mechanisms, fast conformational motion of enzymes relevant for catalytic activity,[45] or the analysis of transition path times.[46] We thus feel that if dye-linker combinations can provide up to $>10^7$ photons per single fluorophore (**20**-ATTO647N, Figure 4), this will pave the way for novel applications of smFRET or other molecular distance rulers.[47]

Acknowledgements

This work was financed by Deutsche Forschungsgemeinschaft (SFB863, project A13; GRK2062, project C03; cluster of excellence CiPSM, LMU excellent to T.C. and SPP 2202 project 422857584 to H.H. and H.L.), an ERC Starting Grant (No. 638536—SM-IMPORT to T.C.), an ERC Advanced Grant (No. 694610—SUPRABIOTICS to A.H.) and by the Center of Nanoscience Munich (CeNS). Parts of the analytical investigations were performed at the Center for Chemical Polymer Technology CPT, which was supported by the European Commission (EUSMI, no. 731019) and the federal state of North Rhine-Westphalia (No. 300088302). STED microscopy was supported by the cluster of excellence NIM and performed at the Center for Advanced Light Microscopy (CALM). L. Zhang thanks the Alexander von Humboldt foundation for a postdoctoral scholarship. M.I. thanks the Life Science Munich graduate school. We thank E. M. Warszawik, Y. Li, L. Kade, N. Gericke, P. Zhou, G. Giacomelli, V. Trauschke and M. Ram for support of this project. We thank Z. J. Mao for providing compound **6**. Open Access funding enabled and organized by Projekt DEAL.

Conflict of Interest

The authors declare no conflict of interest.

Keywords: Biolabelling · Fluorophores · Metal–Chelating Fluorophores · Self-Healing Dyes · Super-Resolution Microscopy

[1] a) M. Schäferling, *Angew. Chem. Int. Ed.* **2012**, *51*, 3532–3554; *Angew. Chem.* **2012**, *124*, 3590–3614; b) T. Ueno, T. Nagano, *Nat. Methods* **2011**, *8*, 642–645.

[2] J. Yao, M. Yang, Y. Duan, *Chem. Rev.* **2014**, *114*, 6130–6178.

[3] L. Zhang, J. Lei, F. Ma, P. Ling, J. Liu, H. Ju, *Chem. Commun.* **2015**, *51*, 10831–10834.

[4] a) G. Hawa, *Application of Fluorescence in Life Sciences for Basic Research and Medical Diagnostics*, Springer, Heidelberg, **2019**, pp. 341–363; b) M. Smilkstein, N. Sriwilaijaroen, X. Kelly Jane, P. Wilairat, M. Riscoe, *Antimicrob. Agents Chemother.* **2004**, *48*, 1803–1806; c) P. O. Krutzik, G. P. Nolan, *Nat. Methods* **2006**, *3*, 361–368.

[5] E. A. Lemke, C. Schultz, *Nat. Chem. Biol.* **2011**, *7*, 480–483.

[6] S. Weiss, *Science* **1999**, *283*, 1676–1683.

[7] a) K. Grußmayer, T. Lukes, T. Lasser, A. Radenovic, *ACS Nano* **2020**, *14*, 9156–9165; b) J. Vogelsang, C. Steinhauer, C. Forthmann, I. H. Stein, B. Person-Skegro, T. Cordes, P. Tinnefeld, *ChemPhysChem* **2010**, *11*, 2475–2490.

[8] J. Liang, J. W. Canary, *Angew. Chem. Int. Ed.* **2010**, *49*, 7710–7713; *Angew. Chem.* **2010**, *122*, 7876–7879.

[9] a) T. Ha, P. Tinnefeld, *Annu. Rev. Phys. Chem.* **2012**, *63*, 595–617; b) J. H. Smit, J. H. M. van der Velde, J. Huang, V. Trauschke, S. S. Henrikus, S. Chen, N. Eleftheriadis, E. M. Warszawik, A. Herrmann, T. Cordes, *Phys. Chem. Chem. Phys.* **2019**, *21*, 3721–3733; c) J. H. M. van der Velde, J. Oelerich, J. Huang, J. H. Smit, A. Aminian Jazi, S. Galiani, K. Kolmakov, G. Gouridis, C. Eggeling, A. Herrmann, G. Roelfes, T. Cordes, *Nat. Commun.* **2016**, *7*, 10144.

[10] a) S. K. Yang, X. Shi, S. Park, T. Ha, S. C. Zimmerman, *Nat. Chem.* **2013**, *5*, 692–697; b) Q. Zheng, A. X. Ayala, I. Chung, A. V. Weigel, A. Ranjan, N. Falco, J. B. Grimm, A. N. Tkachuk, C. Wu, J. Lippincott-Schwartz, R. H. Singer, L. D. Lavis, *ACS Cent. Sci.* **2019**, *5*, 1602–1613; c) J. B. Grimm, L. D. Lavis, *Nat. Methods* **2022**, *19*, 149–158.

[11] a) M. Sauer, J. Hofkens, J. Enderlein, *Handbook of fluorescence spectroscopy and imaging: from ensemble to single molecules*, Wiley-VCH, Weinheim, **2011**; b) J. B. Grimm, B. P. English, J. Chen, J. P. Slaughter, Z. Zhang, A. Revyakin, R. Patel, J. J. Macklin, D. Normanno, R. H. Singer, T. Lionnet, L. D. Lavis, *Nat. Methods* **2015**, *12*, 244–250; c) K. Kolmakov, C. A. Wurm, R. Hennig, E. Rapp, S. Jakobs, V. N. Belov, S. W. Hell, *Chem. Eur. J.* **2012**, *18*, 12986–12998; d) M. Cooper, A. Ebner, M. Briggs, M. Burrows, N. Gardner, R. Richardson, R. West, *J. Fluoresc.* **2004**, *14*, 145–150; e) G. Lukinavičius, K. Umezawa, N. Olivier, A. Honigmann, G. Yang, T. Plass, V. Mueller, L. Reymond, I. R. Corrêa, Jr., Z.-G. Luo, C. Schultz, E. A. Lemke, P. Heppenstall, C. Eggeling, S. Manley, K. Johnsson, *Nat. Chem.* **2013**, *5*, 132–139.

[12] G. G. Dias, A. King, F. de Moliner, M. Vendrell, E. N. da Silva Júnior, *Chem. Soc. Rev.* **2018**, *47*, 12–27.

[13] A. M. Valm, S. Cohen, W. R. Legant, J. Melunis, U. Hershberg, E. Wait, A. R. Cohen, M. W. Davidson, E. Betzig, J. Lippincott-Schwartz, *Nature* **2017**, *546*, 162–167.

[14] S. K. Das, M. D. Austin, M. C. Akana, P. Deshpande, H. Cao, M. Xiao, *Nucleic Acids Res.* **2010**, *38*, e177.

[15] a) M. J. Rust, M. Bates, X. Zhuang, *Nat. Methods* **2006**, *3*, 793–796; b) E. Betzig, H. Patterson George, R. Sougrat, O. W. Lindwasser, S. Olenych, S. Bonifacino Juan, W. Davidson Michael, J. Lippincott-Schwartz, F. Hess Harald, *Science* **2006**, *313*, 1642–1645; c) A. Sharonov, R. M. Hochstrasser, *Proc. Natl. Acad. Sci. USA* **2006**, *103*, 18911–18916.

[16] A. N. Kapanidis, S. Weiss, *J. Chem. Phys.* **2002**, *117*, 10953–10964.

[17] a) F. Chen, P. W. Tillberg, E. S. Boyden, *Science* **2015**, *347*, 543–548; b) G. Wen, M. Vanheusden, V. Leen, T. Rohand, K. Vandereyken, T. Voet, J. Hofkens, *J. Am. Chem. Soc.* **2021**, *143*, 13782–13789; c) G. Wen, M. Vanheusden, A. Acke, D. Valli, R. K. Neely, V. Leen, J. Hofkens, *ACS Nano* **2020**, *14*, 7860–7867.

[18] A. K. Pati, O. El Bakouri, S. Jockusch, Z. Zhou, R. B. Altman, G. A. Fitzgerald, W. B. Asher, D. S. Terry, A. Borgia, M. D. Holsey, J. E. Batchelder, C. Abeywickrama, B. Huddle, D. Rufa, J. A. Javitch, H. Ottosson, S. C. Blanchard, *Proc. Natl. Acad. Sci. USA* **2020**, *117*, 24305–24315.

[19] I. Ugi, *Angew. Chem.* **1959**, *71*, 386–386.

[20] M. A. Fouad, H. Abdel-Hamid, M. S. Ayoup, *RSC Adv.* **2020**, *10*, 42644–42681.

[21] P. Slobbe, E. Ruijter, R. V. A. Orru, *MedChemComm* **2012**, *3*, 1189–1218.

[22] a) I. Ramos-Tomillero, G. Pérez-Chacon, B. Somovilla-Crespo, F. Sánchez-Madrid, C. Cuevas, J. M. Zapata, J. M. Domínguez, H. Rodríguez, F. Albericio, *ACS Omega* **2020**, *5*, 7424–7431; b) T. Ziegler, S. Gerling, M. Lang, *Angew. Chem. Int. Ed.* **2000**, *39*, 2109–2112; *Angew. Chem.* **2000**, *112*, 2202–2205.

[23] a) L. Levi, T. J. J. Müller, *Chem. Soc. Rev.* **2016**, *45*, 2825–2846; b) R. O. Rocha, M. O. Rodrigues, B. A. D. Neto, *ACS Omega* **2020**, *5*, 972–979.

[24] a) C. Besanceney-Webler, H. Jiang, T. Zheng, L. Feng, D. Soriano del Amo, W. Wang, L. M. Klivansky, F. L. Marlow, Y. Liu, P. Wu, *Angew. Chem. Int. Ed.* **2011**, *50*, 8051–8056; *Angew. Chem.* **2011**, *123*, 8201–8206; b) S. I. Presolski, V. P. Hong, M. G. Finn, *Curr. Protoc. Chem. Biol.* **2011**, *3*, 153–162.

[25] S. L. Scinto, D. A. Bilodeau, R. Hincapie, W. Lee, S. S. Nguyen, M. Xu, C. W. am Ende, M. G. Finn, K. Lang, Q. Lin, J. P. Pezacki, J. A. Prescher, M. S. Robillard, J. M. Fox, *Nat. Rev. Methods Primers* **2021**, *1*, 30.

[26] G. Gouridis, G. K. Schuurman-Wolters, E. Ploetz, F. Husada, R. Vietrov, M. de Boer, T. Cordes, B. Poolman, *Nat. Struct. Mol. Biol.* **2015**, *22*, 57–64.

[27] D. P. Nair, M. Podgórski, S. Chatani, T. Gong, W. Xi, C. R. Fenoli, C. N. Bowman, *Chem. Mater.* **2014**, *26*, 724–744.

[28] C. Bös, V. Braun, *FEMS Microbiol. Lett.* **1997**, *153*, 311–319.

[29] a) M. Isselstein, L. Zhang, V. Glembockyte, O. Brix, G. Cosa, P. Tinnefeld, T. Cordes, *J. Phys. Chem. Lett.* **2020**, *11*, 4462–4480; b) M. Schwering, A. Kiel, A. Kurz, K. Lymperopoulos, A. Sprödefeld, R. Krämer, D.-P. Herten, *Angew. Chem. Int. Ed.* **2011**, *50*, 2940–2945; *Angew. Chem.* **2011**, *123*, 2996–3001.

[30] A. Kiel, J. Kovacs, A. Mokhir, R. Krämer, D.-P. Herten, *Angew. Chem. Int. Ed.* **2007**, *46*, 3363–3366; *Angew. Chem.* **2007**, *119*, 3427–3430.

[31] D. Brox, A. Kiel, S. J. Woerner, M. Pernpointner, P. Comba, B. Martin, D.-P. Herten, *PLoS One* **2013**, *8*, e58049.

[32] a) C. Sánchez-Rico, L. Voith von Voithenberg, L. Warner, D. C. Lamb, M. Sattler, *Chem. Eur. J.* **2017**, *23*, 14267–14277; b) S. Ranjit, M. Levitus, *Photochem. Photobiol.* **2012**, *88*, 782–791.

[33] a) J. H. M. van der Velde, J. H. Smit, E. Hebisch, V. Trauschke, M. Punter, T. Cordes, *J. Phys. D* **2019**, *52*, 034001; b) P. Tinnefeld, T. Cordes, *Nat. Methods* **2012**, *9*, 426–427; c) J. H. M. van der Velde, E. Ploetz, M. Hiermaier, J. Oelerich, J. W. de Vries, G. Roelfes, T. Cordes, *ChemPhysChem* **2013**, *14*, 4084–4093; d) J. H. M. van der Velde, J. Oelerich, J. Huang, J. H. Smit, M. Hiermaier, E. Ploetz, A. Herrmann, G. Roelfes, T. Cordes, *J. Phys. Chem. Lett.* **2014**, *5*, 3792–3798; e) J. H. M. van der Velde, J. J. Uusitalo, L.-J. Ugen, E. M. Warszawik, A. Herrmann, S. J. Marrink, T. Cordes, *Faraday Discuss.* **2015**, *184*, 221–235.

[34] a) R. B. Altman, D. S. Terry, Z. Zhou, Q. Zheng, P. Geggier, R. A. Kolster, Y. Zhao, J. A. Javitch, J. D. Warren, S. C. Blanchard, *Nat. Methods* **2012**, *9*, 68–71; b) R. B. Altman, Q. Zheng, Z. Zhou, D. S. Terry, J. D. Warren, S. C. Blanchard, *Nat. Methods* **2012**, *9*, 428–429; c) Q. Zheng, M. F. Juette, S. Jockusch, M. R. Wasserman, Z. Zhou, R. B. Altman, S. C.

Blanchard, *Chem. Soc. Rev.* **2014**, *43*, 1044–1056; d) Q. Zheng, S. Jockusch, Z. Zhou, R. B. Altman, H. Zhao, W. Asher, M. Holsey, S. Mathiasen, P. Geggier, J. A. Javitch, S. C. Blanchard, *Chem. Sci.* **2017**, *8*, 755–762; e) V. Glembockyte, R. Wieneke, K. Gatterdam, Y. Gidi, R. Tampé, G. Cosa, *J. Am. Chem. Soc.* **2018**, *140*, 11006–11012.

[35] a) U. Rothbauer, K. Zolghadr, S. Muyldermans, A. Schepers, M. C. Cardoso, H. Leonhardt, *Mol. Cell. Proteomics* **2008**, *7*, 282–289; b) T. Cordes, A. Maiser, C. Steinhauer, L. Schermelleh, P. Tinnefeld, *Phys. Chem. Chem. Phys.* **2011**, *13*, 6699–6709.

[36] R. J. S. Duncan, P. D. Weston, R. Wrigglesworth, *Anal. Biochem.* **1983**, *132*, 68–73.

[37] X. Ning, R. P. Temming, J. Dommerholt, J. Guo, D. B. Ania, M. F. Debets, M. A. Wolfert, G.-J. Boons, F. L. van Delft, *Angew. Chem. Int. Ed.* **2010**, *49*, 3065–3068; *Angew. Chem.* **2010**, *122*, 3129–3132.

[38] M. L. Blackman, M. Royzen, J. M. Fox, *J. Am. Chem. Soc.* **2008**, *130*, 13518–13519.

[39] K.-T. Chen, C. Ieritano, Y. Seimbille, *ChemistryOpen* **2018**, *7*, 256–261.

[40] J. Liu, Z. Cui, *Bioconjugate Chem.* **2020**, *31*, 1587–1595.

[41] R. Jungmann, C. Steinhauer, M. Scheible, A. Kuzyk, P. Tinnefeld, F. C. Simmel, *Nano Lett.* **2010**, *10*, 4756–4761.

[42] S.-n. Uno, M. Kamiya, T. Yoshihara, K. Sugawara, K. Okabe, M. C. Tarhan, H. Fujita, T. Funatsu, Y. Okada, S. Tobita, Y. Urano, *Nat. Chem.* **2014**, *6*, 681–689.

[43] B. Huang, S. A. Jones, B. Brandenburg, X. Zhuang, *Nat. Methods* **2008**, *5*, 1047–1052.

[44] H. S. Chung, W. A. Eaton, *Curr. Opin. Struct. Biol.* **2018**, *48*, 30–39.

[45] E. J. Loveridge, E. M. Behiry, J. Guo, R. K. Allemann, *Nat. Chem.* **2012**, *4*, 292–297.

[46] B. Schuler, H. Hofmann, *Curr. Opin. Struct. Biol.* **2013**, *23*, 36–47.

[47] a) H. Hwang, H. Kim, S. Myong, *Proc. Natl. Acad. Sci. USA* **2011**, *108*, 7414; b) E. Ploetz, E. Lerner, F. Husada, M. Roelfs, S. Chung, J. Hohlbein, S. Weiss, T. Cordes, *Sci. Rep.* **2016**, *6*, 33257; c) R. Zhou, S. Kunzelmann, M. R. Webb, T. Ha, *Nano Lett.* **2011**, *11*, 5482–5488.

Manuscript received: September 23, 2021
Accepted manuscript online: February 11, 2022
Version of record online: February 26, 2022